We simulated a large-scale thalamocortical network consisting of one million neurons and up to one billion synaptic connections. Parameters of the network are scaled to preserve ratios found in the mammalian thalamocortical system. The white matter anatomy of the model is reconstructed from human diffusion tensor imaging (DTI) data using fiber-tracktography methods. The gray-matter anatomy consists of 5 cortical layers with microcircuitry of a "generic primary sensory area" and specific, non-specific, and reticular thalamic nuclei. The model has 12 types and numerous subtypes of neurons with multi-compartment dendritic trees; synapses with AMPA, NMDA, GABA$_A$, GABA$_B$, and gap-junction kinetics; axonal lengths and conduction delays; synaptic short-term depression and facilitation; synaptic long-term spike-timing-dependent plasticity (STDP); and neuromodulation derived from the brainstem dopaminergic reward system. The parameters of the model are taken from the published literature, mostly on cat area 17 and lamina A of dorsal thalamus. In some cases, a number of arbitrary but justifiable choices had to be made.

As compared to real cortex, the model has a scaled down density of neurons and synapses per mm^2 of cortical surface. Model neurons have scaled down number of synapses and impoverished dendritic trees in comparison with real cortical neurons. Moreover, we do not model subcortical structures other than the thalamus. We do not model developmental changes other than that reflected in activity-dependent fine-tuning of connectivity.

Most simulations were performed with one million neurons, though a variant of the model was simulated with 10^{11} neurons and almost one quadrillion synapses, which corresponds to the full size of the human brain. Movies of the simulation are available on the first author website (`http://www.izhikevich.com`).

1   Anatomy

1.1   Microcircuitry

Neurons in the model are either excitatory (glutamatergic, red in Fig. 8) or inhibitory (GABAergic, blue or green in Fig. 8). We adapt the nomenclature of [1] and distinguish the following types of cortical excitatory neurons:

p2/3	pyramidal neurons in L2/3
ss4(L4)	spiny stellate neurons in L4 that project to L4
ss4(L2/3)	spiny stellate neurons in L4 that project to L2/3
p4	pyramidal neurons in L4
p5(L2/3)	pyramidal neurons in L5 that project to L2/3
p5(L5/6)	pyramidal neurons in L5 that project to L5/6
p6(L4)	pyramidal neurons in L6 that project to L4
p6(L5/6)	pyramidal neurons in L6 that project to L5/6

Pyramidal neurons exhibit regular spiking (RS) firing patterns (Connors and Gutnick 1990), but can also exhibit chattering (CH, or fast rhythmic bursting FRB) pattern or intrinsically bursting (IB) pattern, which we describe in detail below.

We distinguish two types of cortical GABAergic (inhibitory) interneurons

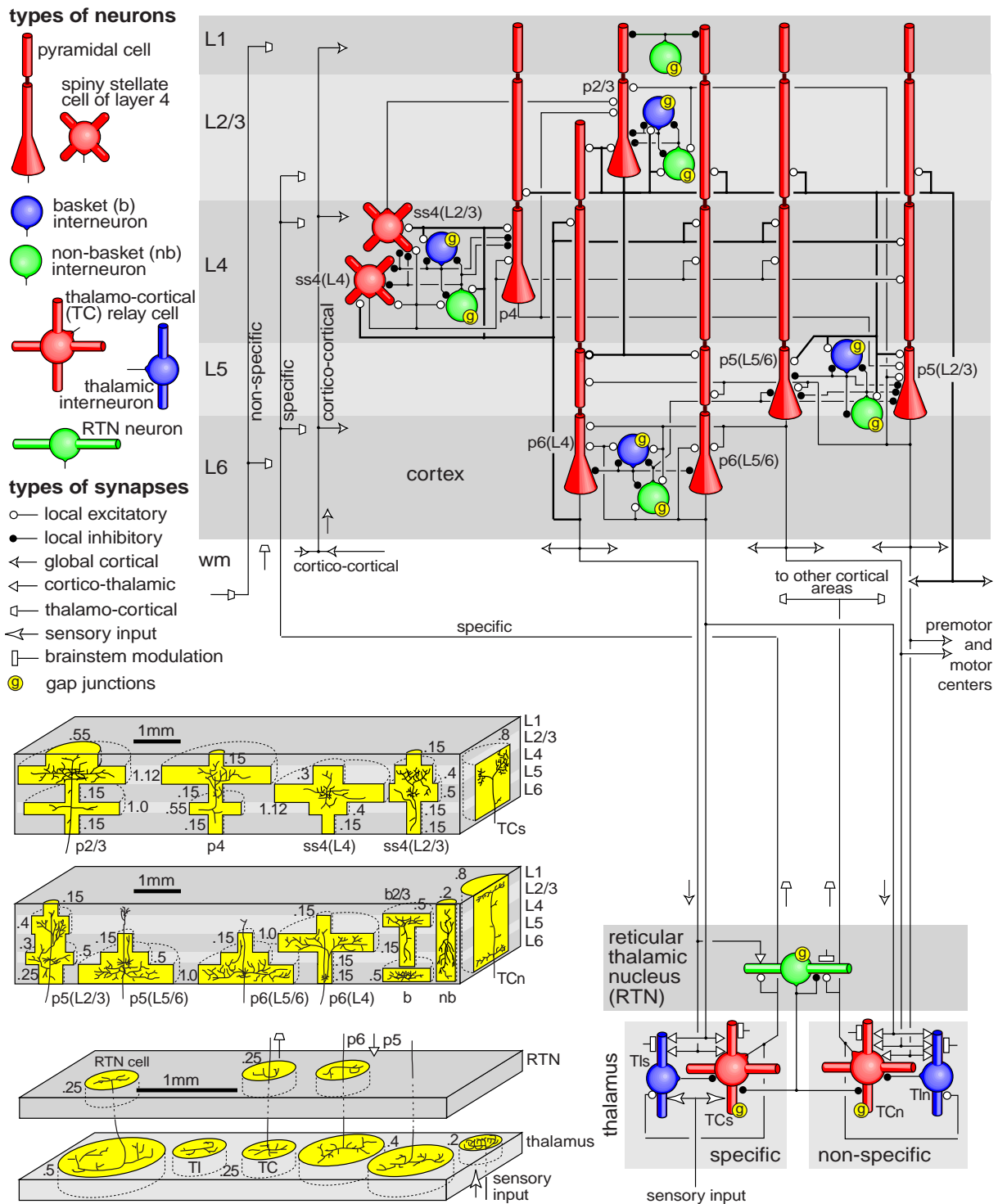|	
b	basket interneuron, all layers
nb	non-basket interneuron, all layers

Figure 8: Simplified diagram of thalamocortical microcircuit. Only the most significant or numerous connections are shown; see Fig. 9 for details. Self-synapses denote synaptic connections within the populations. Bold lines denote pathways carrying more than 30% of synapses to a particular target.

Basket cells have fast spiking (FS) firing patterns [2]. Non-basket interneurons morphologically include double-bouquet cells, neurogliaform cells, and Martinotti cells [1], and they can exhibit LTS (low-threshold spiking, [3]), LS (latent spiking), RSNP (regular spiking non-pyramidal neurons) or BSNP (burst spiking non-pyramidal neurons) firing patterns [4, 5], and a diversity of other patterns [6], as we explain the next section. In the model, basket interneurons in L4, L5, and L6 have axons confined within a single cortical layer, whereas basket cells in L2/3 and non-basket interneurons may have axons spanning several layers [7, 8].

We distinguish three thalamic nuclei with three cell types:

TCs	thalamocortical relay neurons in specific nucleus
TCn	thalamocortical relay neurons in non-specific nucleus
TIs	thalamic interneurons in specific nucleus
TIn	thalamic interneurons in non-specific nucleus
RTN	GABAergic neurons in the reticular thalamic nucleus

We do not make the distinction between X and Y thalamocortical relay neurons [9]. TC and RTN cells exhibit regular spiking or bursting patterns depending on the holding potential.

The relative distribution (percentage) of neuronal types in the model is given in the first column in Fig. 9. It is based on the following published data: The relative number of cortical neurons in different layers in the primary visual cortex was given by [1], Fig. 6). Consistent with earlier studies, they found that inhibitory neurons form approximately 20% of all neurons. The relative number of basket and non-basket cells is consistent with earlier studies (Fig. 4 of [10], Fig. 1 of 5). The relative number of neurons in the thalamic nuclei is not known. Peters and Payne [11] report 350,000 thalamocortical fibers per 11,000,000 neurons in L4 of area 17 [1], resulting in a ratio of 1/30, which is consistent with other observations [12]. Assuming one such fiber per TC cell, we derive the number of TC cells as a fraction of L4 neurons. Winer and Larue [13] report 20% of interneurons in LGN of rats, cats, and monkeys, but different percentages in other nuclei. We assume here that exactly 20% of neurons in the specific and non-specific thalamic nuclei are inhibitory interneurons. Not knowing the number of RTN neurons, we take it to be the same as the number of TC neurons in each nucleus. Notice that the majority of neurons in the model are in L2/3, L4 and L6.

Making three-dimensional reconstructions of 39 single neurons and thalamic afferents in cat primary visual cortex (area 17), Binzegger et al. [1] characterized the distribution of all synapses formed on each neuronal type at each cortical layer, see Fig. 7 in their paper. The authors kindly provided us with their data files, which were used to obtain the cortical part of the table in Fig. 9. We treat 95% of the unidentified asymmetrical (excitatory) synapses in L1-L6 as coming from other cortical areas (corticocortical) and 5% as coming from the non-specific thalamic nucleus. We treat the unidentified symmetrical (inhibitory) synapses as coming from non-basket cells. Converting the absolute values into percentages, we assign synapses in the model with the distribution in shown in the table in Fig. 9.

The table also reflects the relative distribution of synapses in the thalamus, which is based on the numbers found in the A-laminae of the LGN of the cat. van Horn et al. [14] found that TC neurons in LGN receive 7.1% synapses from sensory (retinal) fibers, 62% excitatory synapses from cortex (L5 and L6) and brainstem (divided equally between the two, see Erisir et al. 1997 and 30.9% GABAergic synapses. Thalamic interneurons receive 48.7% synapses from sensory fibers, 24.4% GABAergic synapses, and the

Figure 9: Distribution of neuronal types and synapses in the model. Each row represents a single postsynaptic neuron of a certain type. Multiple compartments, if they exist, are indicated. Each element in a row represents the percentage of synapses of a particular type to that neuron. The most significant connections are shown in Fig. 8. Shaded regions denote plastic connections.

rest are from cortex and brainstem. Since there are four types of cortical pyramidal neurons projecting to thalamus, we assume that the distribution of cortico-thalamic synapses in the thalamus is proportional to the relative distribution of the cortical neurons. We assume that RTN neurons are qualitatively similar to TC neurons with respect to the number of brainstem synapses, cortico-thalamic synapses, etc.

Notice that the table has very few zero (empty) entries; for the sake of clarity, we depict only the most significant or numerous connections in Fig. 8. Bold lines in the figure denote projections from p2/3 and p6(L4) that carry the majority of synaptic input (more than 30% each) to their targets. The proportion of thalamocortical synapses is small, but the synapses are quite strong, as we discuss in the next section.

Generalizing the interneuron circuitry of L4 of barrel somatosensory cortex of rats ([3]; Michael Beierlein and Jay Gibson, personal communication) we assume that the connectivity of interneurons is the same in all cortical layers: There are gap-junction (electrical) synapses among neurons of the same type at each layer and no gap junctions between neurons belonging to different types. Landisman et al. [15] report gap junctions among RTN neurons in mice and rats, but no chemical synapses. In contrast, [16] and [17] report GABAergic synapses in the same neurons. We include both types of synapses in the model of the thalamic reticular nucleus. Hughes et al. [18] report gap junctions among TC relay neurons. Since no evidence exists of any chemical synapses among the neurons [12], only electrical synapses among TC cells are modeled in this study.

Typical axonal arborizations of various neuronal types are illustrated in Fig. 8, lower-left. The magnitudes of the laminar axonal spread of cortical neurons are based on the macaque striate cortex data of [19] and [20], which are consistent with cat area 17 data of [1]. Thalamic neurons are from [21] and reticular neurons are from [22] and [15]. Sur et al. [23] report the diameter of cat retino-geniculate arborizations to be 0.15 mm for X-type and 0.3 mm for Y-type, whereas [24] report slightly larger estimates. We take the radius of sensory fibers in the model to be 0.2 mm. Murphy and Sillito [25] report the spread of L6 cortico-thalamic arborizations to be 0.5 mm with some fibers spreading as much as 1.5 mm. We assume that the radius of thalamic arborization of all cortical axons is 0.4 mm. Jones ([12], Fig.3.9) reports the spread of thalamocortical fibers to be around 0.4 mm for X-type and 0.8 mm for Y-type with multiple synaptic clusters. Since we do not distinguish the types, we take the larger number and keep in mind that there will be activity-dependent pruning.

Yellow circles in Fig. 8 with indicated radii (mm) denote the initial axonal spans used in the model. The synaptic density decays linearly from the center of the circle to a zero value at the edge.

1.2   White Matter Anatomy (After Human DTI)

The gross anatomy of long-range corticocortical connections in the model is based on the anatomy of the human brain obtained via anatomical MRI and DTI scans. Neuronal bodies are allocated randomly on the cortical surface, whose coordinates were obtained from anatomical MRI. Local-circuit connectivity is established according to Fig. 8 and table in Fig. 9. The axons that exit the gray matter and enter the white matter are directed according to the "TensorLine" method ([26, 27]) applied to human DTI scans; see Fig. 1 of the main text. Once the axon re-enters the gray matter (in some distal part of the cortex), it ramifies according to the distances in Fig. 8.

Axons of each pyramidal neuron in layer 2/3 in the model bifurcates into ipsilateral and contralateral axons. The former are continued according to the DTI data, and the latter project to the mirror locations

in the contralateral hemisphere. Because human hemispheres are not symmetrical, the target point for the axon is found on the contralateral hemisphere that is closest to the mirror location of the neuron.

Each thalamocortical neuron in the non-specific thalamic nuclei projects to a random location on cortex. The specific nuclei are assumed to have the form of two hemispheres and thalamocortical neurons there project roughly topographically to corresponding locations in the cortex. To deliver visual, auditory, or somatosensory signals, we stimulate corresponding neurons in the specific thalamic nuclei that project to the visual, auditory, and somatosensory areas of the cortex.

To have a sufficiently large density of neurons per mm^2 of cortical surface, we scaled down the entire structure by a factor of 4. That is, we assumed that the cortex is 40mm wide, i.e., it can be embedded within a sphere with diameter of 40mm. The length of the traced fibers is used to estimate the axonal conduction delays as follows: For corticocortical connections, we assume that the axonal conduction velocity is 1m/s for myelinated fibers and 0.1 m/s for non-myelinated fibers (28–30]. The cortex is assumed to have 1 mm width, so a delay from layer 6 to layer 1 could be as large as 10ms. Delays via myelinated (in white matter) and non-myelinated (in gray matter) fibers are added to find the total conduction delay. The delays from layer 5 to thalamus are taken to be 1 ms and from layer 6 to thalamus are taken to be 20 ms. Delays from specific thalamocortical neurons are taken to be 1 ms. Delays from non-specific thalamocortical cells are determined according to the length of the axonal fiber. If the resulting conduction delay of any neuron is longer than 20 ms, it is reduced to exactly 20 ms to have an efficient implementation algorithm (this number is a parameter in the model, and it can be easily changed; we used 20ms for all our simulations).

Sensory input to the model is delivered via stimulation of the thalamocortical neurons (TCs) projecting to the appropriate primary sensory cortex (appropriate sensory modality). In particular, to deliver auditory, visual, or somatosensory stimulation, we inject brief pulses of current into TCs neurons in the MGN, LGN, and VPN nuclei of thalamus.

2 Dynamics

The large-scale model consists of various types of multi-compartmental neurons with active dendrites, synaptic transmission with AMPA, GABA, and NMDA kinetics, and short-term and long-term synaptic plasticity with dopaminergic modulation.

2.1 Neuronal Dynamics

Spiking dynamics of each neuron (and each dendritic compartment) were simulated using the phenomenological model proposed by Izhikevich [31]. The model has only 2 equations and 4 dimensionless parameters that could be explicitly found from neuronal resting potential, input resistance, rheobase current, and other measurable characteristics ([32], chapter 8). We present the model in a dimensional form so that the membrane potential is in millivolts, the current is in picoamperes and the time is in milliseconds:

$$C\dot{v} = k(v - v_{\mathrm{r}})(v - v_{\mathrm{t}}) - u + I \tag{1}$$

$$\dot{u} = a\{b(v - v_{\mathrm{r}}) - u\} \tag{2}$$

where C is the membrane capacitance, v is the membrane potential (in mV), v_{r} is the resting potential, v_{t} is the instantaneous threshold potential, u is the recovery variable (the difference of all inward and outward

voltage-gated currents), I is the dendritic and synaptic current (in pA)

$$I(t) = -I_{\text{dendr}} - I_{\text{syn}}$$

as explained below, a and b are parameters. When the membrane potential reaches the peak of the spike, i.e., $v > v_{\text{peak}}$, the model is said to fire a spike, and all variables are reset according to $v \leftarrow c$ and $u \leftarrow u+d$, where c and d are parameters. Notice that v_{peak} (typically around +50 mV) is not a threshold but is rather a peak of the spike; the firing threshold in the model (as in real neurons) is not a parameter but a dynamic property that depends on the state of the neuron.

Depending on the values of the parameters, the model could be tuned to reproduce firing dynamics of every known cortical, thalamic, and hippocampal neuron ([32). We illustrate some of the firing patterns in Fig. 10 using injected pusles of somatic current (see Fig. 8.17 in [32] for in vivo-like input). It is different from the Hodgkin-Huxley-type models in the sence that it reproduces the responses, and not the ionic currents, of biological neurons.

Each neuron has a somatic compartment and a set of dendritic compartments. The number of dendritic compartments of a neuron in each cortical layer is at least $S*\text{scale}/M$ where S is the number of synapses the neuron receives in the layer (see Fig. 9), scale= 0.05 is the scale-down factor when we simulate fewer than 10^{11} neurons, and the parameter $M = 40$ is the maximal number of synapses per compartment. The dendritic current at each compartment consists of the currents coming from the *down* ("mother") compartment (zero for somatic compartments) and *up* ("daughter") compartments (zero for terminal compartments)

$$I_{\text{dendr}} = G_{\text{down}}(V - V_{\text{down}}) + \sum_{\text{up}} G_{\text{up}}(V - V_{\text{up}})$$

with the values of the conductances G_{up} and G_{down} provided in Fig. 10.

2.2 Synaptic Dynamics

We model synaptic dynamics in a fashion similar to that by Izhikevich et al. [33] with the exception that we use a simpler and more efficient model for short-term synaptic plasticity, and spike-timing-dependent plasticity (STDP) is considered to be modulated by dopamine.

Short-Term Synaptic Plasticity. We assume that the synaptic conductance (strength) of each synapse can be scaled down (depression) or up (facilitation) on a short time scale (hundreds of milliseconds) by a scalar factor x. This scalar factor, different for each presynaptic cell, is modeled by the following one-dimensional equation

$$\dot{x} = (1 - x)/\tau_x , \qquad x \leftarrow px \quad \text{when presynaptic neuron fires.} \tag{3}$$

That is, x tends to recover to the equilibrium value $x = 1$ with the time constant τ_x, and it is reset by each spike of the presynaptic cell to the new value px. Any value $p < 1$ decreases x and results in short-term synaptic depression, whereas $p > 1$ results in short-term synaptic facilitation, as we illustrate in Fig. 11.
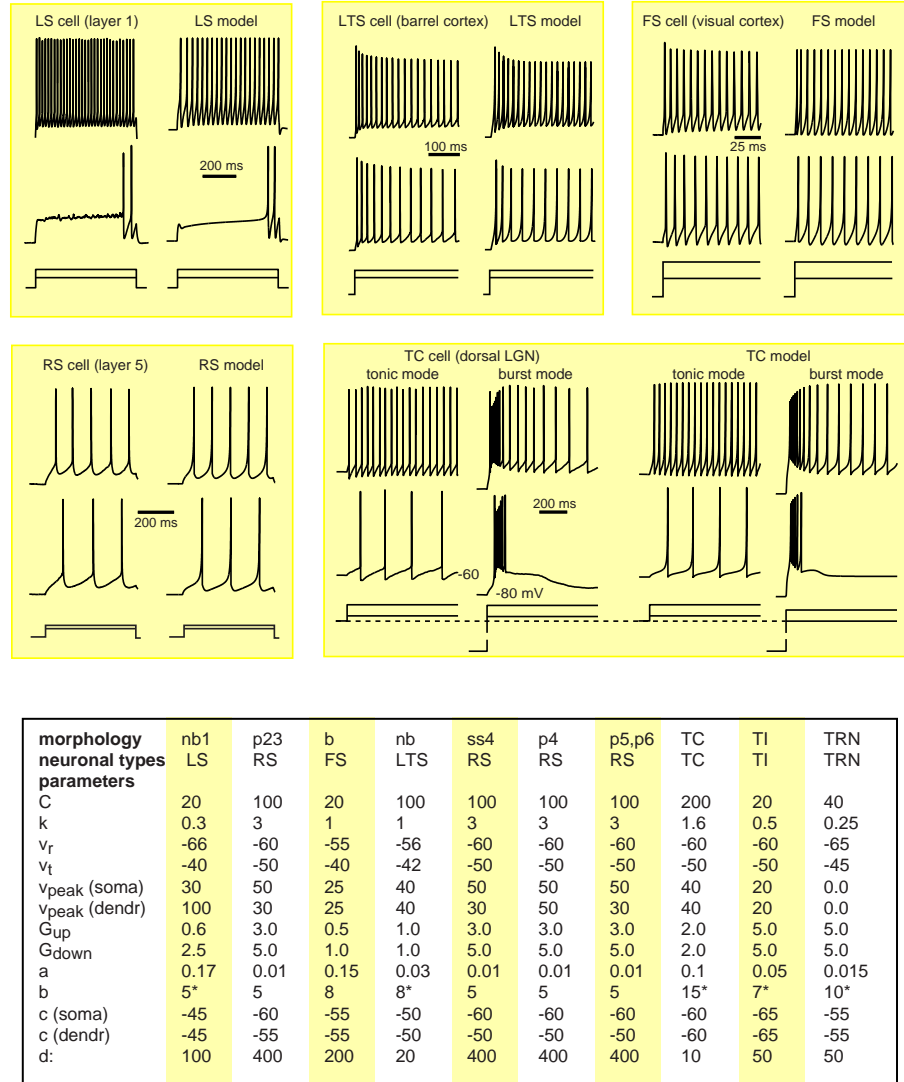
morphology	nb1	p23	b	nb	ss4	p4	p5,p6	TC	TI	TRN
neuronal types	LS	RS	FS	LTS	RS	RS	RS	TC	TI	TRN
parameters										
C	20	100	20	100	100	100	100	200	20	40
k	0.3	3	1	1	3	3	3	1.6	0.5	0.25
v_r	-66	-60	-55	-56	-60	-60	-60	-60	-60	-65
v_t	-40	-50	-40	-42	-50	-50	-50	-50	-50	-45
v_{peak} (soma)	30	50	25	40	50	50	50	40	20	0.0
v_{peak} (dendr)	100	30	25	40	30	50	30	40	20	0.0
G_{up}	0.6	3.0	0.5	1.0	3.0	3.0	3.0	2.0	5.0	5.0
G_{down}	2.5	5.0	1.0	1.0	5.0	5.0	5.0	2.0	5.0	5.0
a	0.17	0.01	0.15	0.03	0.01	0.01	0.01	0.1	0.05	0.015
b	5*	5	8	8*	5	5	5	15*	7*	10*
c (soma)	-45	-60	-55	-50	-60	-60	-60	-60	-65	-55
c (dendr)	-45	-55	-55	-50	-50	-50	-50	-60	-65	-55
d:	100	400	200	20	400	400	400	10	50	50

Figure 10: Comparison between in vitro recordings of various neurons and their simulations in the large-scale model. Different neuronal types are modeled by the same equations 1 and 2 but with different choice of parameters. $*$: Dendritic compartments of the LS neuron are modeled as a passive compartment $\dot{v} = (-I_{\mathrm{dendr}} - I_{\mathrm{syn}})/250$. For LTS neurons, the recovery variable is kept below the value of 670; that is, if $u > 670$, then $u = 670$. For TI neurons, if $u > 530$, then $u = 530$. For TC and TRN neurons, the value b is voltage-dependent: if $v > -65$, then $b = 0$ for TC and $b = 2$ for TRN.
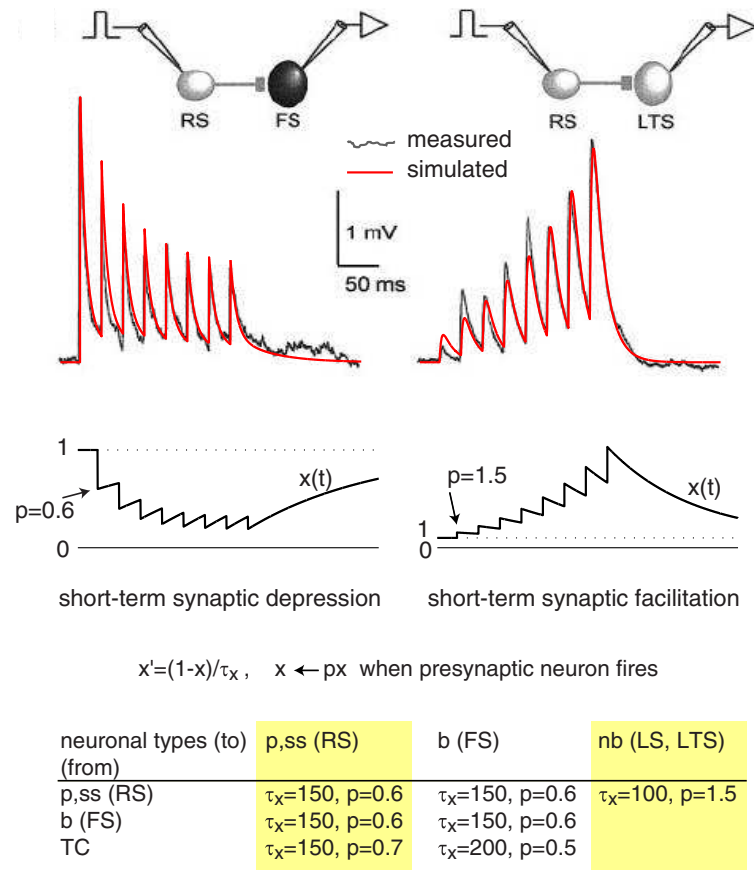
Figure 11: Short-term synaptic depression and facilitation is modeled by the one-dimensional equation 3 with two parameters, τ_x and p. Top: comparison of experimentally measured (Fig. 4 from [3]) and simulated synaptic dynamics. Bottom: values of parameters used in the large-scale model. Other synaptic connections, e.g., from nb (LTS) cells, are assumed not to have short-term plasticity.

Synaptic Kinetics. The total synaptic current at each compartment is simulated as

$$I_{\text{syn}} \quad = \quad g_{\text{AMPA}}(v - 0) + g_{\text{NMDA}} \frac{[(v + 80)/60]^2}{1 + [(v + 80)/60]^2}(v - 0)$$
$$+ g_{\text{GABA}_\text{A}}(v + 70) + g_{\text{GABA}_\text{B}}(v + 90) \quad + \quad I_{\text{gap}}$$

where v is the postsynaptic membrane potential, and the subscript indicates the receptor type. Each conductance g (here we omit the subscript for the sake of clarity) has first-order linear kinetics

$$\dot{g} = -g/\tau$$

with $\tau =$ 5, 150, 6, and 150 ms for the simulated AMPA, NMDA, GABA$_A$ and GABA$_B$ receptors, respectively [34, 33].

The ratio of NMDA to AMPA receptors was set to be uniform at a value of 1 for all excitatory neurons. Thus, each firing of an excitatory neuron increases g_{AMPA} and g_{NMDA} by xc, where c is the synaptic conductance (synaptic weight) and x is the short-term depression/potentiation scaling factor as above. Similarly, the value of GABA$_A$ to GABA$_B$ receptors is taken to be 1 for all inhibitory synapses.

The gap-junction (electrical synapse) current

$$I_{\text{gap}} = \sum_{i \in \text{neighbors}} g_i(v - v_i)$$

has conductance decaying with the distance from the neuronal soma to the neighboring neuron i. Evaluation of the gap-junction currents is extremely costly from a computational point of view, since they need to be evaluated pair-wise for all neurons at all time steps, and most of the results presented in the paper were performed with $g_i = 0$ (unless mentioned otherwise).

Dopamine-modulated dendritic STDP. The conductance (weight) of each synapse in the model is simulated according to spike-timing-dependent plasticity (STDP): The synapse is potentiated or depressed depending on the order of firing of the presynaptic neuron and the corresponding (dendritic or somatic) compartment of the postsynaptic neuron (35, 36, 37, 38). We use equations in the form provided by 32 so that STDP could be modulated by dopamine. In particular, we use the parameters $A_+ = 1$, $A_- = 2$, $\tau_+ = \tau_- = 20$ ms (see [39 or 40]) so that the depression area of the STDP function is twice as large as the potentiation area.

Since dendritic compartments can generate spikes independently from the soma, synapses could be potentiated or depressed even in the absence of spiking of the postsynaptic cell. We keep the synaptic conductance within the range $[0, s_{\text{max}}]$, where s_{max} is 10.0 if the presynaptic cell is of pyramidal (p) or spiny stellate (ss) type, 20.0 if the presynaptic cell is of thalamocortical (TC) type, 6.0 if the presynaptic cell is of basket (b) type, 4.0 if the presynaptic cell is of non-basked (nb) type, and 5.0 if the presynaptic cell is of thalamic inhibitory (TI) or reticular thalamic nucleus (RTN) type. All GABAergic synapses in the model are assumed to be non-plastic and their conductance is fixed at the value of 4.0. The initial values of the glutamatergic synapses are random drawn from the uniform distribution on the interval $[0, 6]$, and then they evolve according to STDP.

In most cases, firing of an excitatory presynaptic neuron can evoke a local EPSP in the dendritic compartment of the postsynaptic cell of less than 10 mV amplitude, which typically results in submillivolt EPSP at the somatic compartment due to the electrotonic attenuation of synaptic current. Coincident firing of three or four synapses with the maximal conductances *in the same compartment* may result in a local dendritic spike, which then could propagate to the soma and evoke a spike or burst response there. Such spikes arriving at different compartments would not be as effective in evoking the somatic response.

3   Intracranial EEG

We assume that the intracranial EEG (iEEG) at any cortical location is the sum of all extracellular currents generated by nearby neurons within a sphere of radius of 1.5 mm, so it is essentially the sum of local field potentials. These currents are mostly the intracellular currents flowing across vertically aligned apical dendrites of pyramidal cells. The basal dendrites of pyramidal cells and the dendritic trees of the other types of neurons are not aligned; they may generate many strong currents, but the currents flow at random directions and thereby cancel each other.

4   Simulated fMRI/BOLD

We simulate fMRI/Blood Oxygenation Level Dependent (BOLD) signal [41] at each region (voxel) as the sum of all synaptic activity (all synaptic conductances) of all neurons within the region

$$\dot{y} = (\text{total synaptic conductance}) - y/500 .$$

Thus, we assume that the major source for metabolic demand in the model is the synaptic transmission.

Acknowledgment

References

1. Binzegger T., Douglas R.J., Martin K.A.C. (2004) A Quantitative Map of the Circuit of Cat Primary Visual Cortex. Journal of Neuroscience, 24:8441–8453.

2. Connors B.W and Gutnick M.J. (1990) Intrinsic firing patterns of diverse neocortical neurons. Trends in Neuroscience, 13:99–104.

3. Beierlein M., Gibson J.R., and Connors B.W. (2003) Two Dynamically Distinct Inhibitory Networks in Layer 4 of the Neocortex. Journal of Neurophysiology, 90:2987–3000.

4. Kawaguchi Y. (1995) Physiological Subgroups of Nonpyramidal Cells with Specific Morphological Characteristics in Layer II/III of Rat Frontal Cortex. Journal of Neuroscience, 15:2638–2655.

5. Kawaguchi Y. and Kubota Y. (1997) GABAergic Cell Subtypes and their Synaptic Connections in Rat Frontal Cortex. 7:476–486.

6. Markram H., Toledo-Rodriguez M., Wang Y., Gupta A., Silberberg G., and Wu C. (2004) Interneurons of the Neocortical Inhibitory System. Nature Reviews Neuroscience, 5:793–807.

7. Kubota Y. and Kawaguchi Y. (2000) Dependence of GABAergic Synaptic Areas on the Interneuron Type and Target Size. Journal of Neuroscience. 20:375–386.

8. Xiang Z., Huguenard J.R., and Prince D.A. (1998) Cholinergic Switching Within Neocortical Inhibitory Networks. Science, 281:985–988.

9. Sherman S.M. and Guillery R.W. (2004) Thalamus. In Shepherd G.M. (Ed.) The Synaptic Organization of the Brain. Oxford University Press.

10. Amitai Y., Gibson J.R., Beierlein M., Patrick S.L., Ho A.M., Connors B.W. (2002) The Spatial Dimensions of Electrically Coupled Networks of Interneurons in the Neocortex. Journal of Neuroscience, 22:4142–4152.

11. Peters A. and Payne B.R. (1993) Numerical relationships between geniculocortical afferents and pyramidal cell modules in cat primary visual cortex. Cerebral Cortex, 3:69–78

12. Jones, E.G. (1985) The Thalamus, New York: Plenum Press.

13. Winer J.A. and Larue D.T. (1996) Evolution of GABAergic circuitry in the mammalian medial geniculate body. PNAS 93:3083–3087.

14. van Horn S.C., Erisir A. and Sherman S.M. (2000) Relative Distribution of Synapses in the A-Laminae of the Lateral Geniculate Nucleus of the Cat. J. Compar. Neurology, 416:509–520.

15. Landisman C.E., Long M.A., Beierlein M., Deans M.R., Paul D.L., and Connors B.W. (2002) Electrical Synapses in the Thalamic Reticular Nucleus. Journal of Neuroscience, 22:1002–1009.

16. Zhang S.J., Huguenard J.R., Prince D.A. (1997) $GABA_A$ Receptor-Mediated Cl^- Currents in Rat Thalamic Reticular and Relay Neurons. JOurnal of Neurophysiology, 78:2280–2286.

17. Sohal V.S., Huntsman M.M., and Huguenard J.R. (2000) Reciprocal Inhibitory Connections REgulate the Spatiotemporal Properties of Intrathalamic Oscillations. Journal of Neuroscience, 20:1735–1745.

18. Hughes SW, Blethyn KL, Cope DW, and Crunelli V. (2002) Properties and origin of spikelets in thalamocortical neurones in vitro. Neuroscience 110:395–401

19. Blasdel G.G., Lund J.S., Fitzpatrick D. (1985) Intrinsic Connections of Macaque Striate Cortex: Axonal Projections of Cells Outside Lamina 4C. Journal of Neuroscience, 5:3350–3369.

20. Fitzpatrick D., Lund J.S., Blasdel G.G. (1985) Intrinsic Connections of Macaque Striate Cortex: Afferent and Efferent Connections of Lamina 4C. Journal of Neuroscience, 5:3329–3349.

21. Yen C.T., Conley M., Hendry .S.H.C., Jones E.G. (1985) The Morphology of Physiologically Identified GABAergic Neurons in the Somatic Sensory Part of the Thalamic Reticular Nucleus in the Cat. JOurnal of Neuroscience, 5:2254–2268.

22. Cox C.L., Huguenard J.R., and Prince D.A. (1997) Nucleus reticularis neurons mediate diverse inhibitory effects in thalamus. PNAS, 94:8854–8859.

23. Sur M., Esguerra M., Garraghty P.E., Kritzer M.F., and Sherman S M. (1987) Morphology of Physiologically Identified Retinogeniculate X- and Y-Axons in the Cat. Journal of Neurophysiology, 58:1–32.

24. Bowling D.B. and Michael C.R. (1994) Terminal Patterns of Single, Physiologically Characterized Optic Tract Fibers in the Cat's Lateral Geniculate Nucleus. Journal of Neuroscience, 4:198–216.

25. Murphy P.C. and Sillito A.M. (1996) Functional Morphology of the Feedback Pathway from Area 17 of the Cat Visual Cortex to the Lateral Geniculate Nucleus. Journal of Neuroscience, 16:1180–1192.

26. Weinstein D., Kindlmann G., Lundberg E. (1999) Tensorlines: advection-diffusion based propagation through diffusion tensor fields. IEEE Proceedings of the conference on Visualization'99. p. 249 - 253

27. Mori S. and van Zijl P.C.M. (2002) Fiber tracking: principles and strategies - a technical review. NRM in Biomedicine, 15:468-480.

28. Swadlow H. A. (1991) Efferent neurons and suspected interneurons in second somatosensory cortex of the awake rabbit: receptive fields and axonal properties. J Neurophysiol 66: 1392-1409

29. Swadlow H. A. (1992) Monitoring the excitability of neocortical efferent neurons to direct activation by extracellular current pulses. J Neurophysiol 68: 605–619

30. Swadlow H.A. (1994) Efferent Neurons and Suspected Interneurons in Motor Cortex of the Awake Rabbit: Axonal Properties, Sensory receptive Fields, and Subthreshold Synaptic Inputs. Journal of Neurophysiology, 71: 437-453.

31. Izhikevich E. M. (2003) Simple Model of Spiking Neurons. IEEE Transactions on Neural Networks, 14:1569-1572

32. Izhikevich E. M. (2007) Dynamical Systems in Neuroscience: The Geometry of Excitability and Bursting. The MIT Press

33. Izhikevich E.M., Gally J.A., and Edelman, G.M. (2004) Spike-Timing Dynamics of Neuronal Groups. Cerebral Cortex, 14:933-944

34. Dayan P. and Abbott L. F. (2001) Theoretical Neuroscience: Computational and Mathematical Modeling of Neural Systems. The MIT Press, Cambridge, MA

35. Levy W.B. and Steward O. (1983) Temporal contiguity requirements for long-term associative potentiation/depression in the hippocampus. Neuroscience, 8:791–797

36. Gerstner W., Kempter R., van Hemmen J. L., Wagner H. (1996) A neuronal learning rule for sub-millisecond temporal coding Nature, 383: 76 - 78

37. Markram, H., Lubke, J., Frotscher, M. and Sakmann, B. (1997). Regulation of synaptic efficacy by coincidence of postsynaptic APs and EPSPs. Science, 275, 213-215.

38. Bi, G.Q., and Poo, M.M. (1998). Synaptic modifications in cultured hippocampal neurons: dependence on spike timing, synaptic strength, and postsynaptic cell type. J. Neurosci. 18, 10464-10472.

39. Izhikevich E.M. and Desai N.S. (2003) Relating STDP to BCM. Neural Computation 15:1511-1523

40. Izhikevich E.M. (2006) Polychronization: Computation With Spikes. Neural Computation,18:245-282

41. Ogawa S. and Sung Y.-W. (2007) Functional Magnetic Resonance Imaging. Scholarpedia, 2: 3105